2022

Two-Component 3D Atomic Bose-Einstein Condensates Support Complex Stable Patterns

N. Boullé

I. Newell

P. E. Farrell

Panayotis G. Kevrekidis

Two-Component 3D Atomic Bose-Einstein Condensates Support Complex Stable Patterns

N. Boullé,[1,*] I. Newell,[1,†] P. E. Farrell,[1,‡] and P. G. Kevrekidis[2,§]

[1] *Mathematical Institute, University of Oxford, Oxford OX2 6GG, United Kingdom*
[2] *Department of Mathematics and Statistics, University of Massachusetts Amherst, Amherst, MA 01003-4515, USA*

(Dated: August 12, 2022)

We report the computational discovery of complex, topologically charged, and spectrally stable states in three-dimensional multi-component nonlinear wave systems of nonlinear Schrödinger type. While our computations relate to two-component atomic Bose-Einstein condensates in parabolic traps, our methods can be broadly applied to high-dimensional, nonlinear systems of partial differential equations. The combination of the so-called deflation technique with a careful selection of initial guesses enables the computation of an unprecedented breadth of patterns, including ones combining vortex lines, rings, stars, and "vortex labyrinths". Despite their complexity, they may be dynamically robust and amenable to experimental observation, as confirmed by Bogolyubov-de Gennes spectral analysis and numerical evolution simulations.

Introduction.—The realm of nonlinear Schrödinger models has been one of the principal pillars for the study of nonlinear wave phenomena in dispersive systems [1–4]. The relevant applications span a wide range of fields including nonlinear optical systems [5], water waves and plasmas [6], as well as importantly over the last two decades, the atomic physics setting of Bose–Einstein condensates (BECs) [7, 8]. In the latter setting, nonlinear structures in the form of bright [9] and dark [10] solitary waves, but also importantly topologically charged patterns in the forms of vortices [11, 12] in two dimensions (2D), as well as vortex rings, lines or knots, among others [13–15] in three dimensions (3D) have played a central role not only in theoretical and computational, but also in experimental studies. Indeed, these have been connected to notions such as persistent currents [16], turbulence and associated cascades [17], emulations of an expanding universe in the lab [18], as well as Hawking radiation from analogue black holes [19].

While the majority of the relevant contributions focused on single-component systems, such as single atomic species BECs, gradually this situation is changing. Over the past few years, it has been realized that coupled systems can be exploited to manipulate the spin degree of freedom [20] in order to produce a wide variety of topological and non-topological, ground and excited state coherent structures, both in one dimension (1D) [21] and higher dimensions [22]. However, developing numerical methods to compute nonlinear waveforms in high dimensions, such as 3D, poses considerable challenges, even in single-component settings [23, 24]. This is even harder in multi-component systems, where only a few groups have attempted to provide a description of stability of singular and non-singular patterns featuring vortices, monopoles, and the so-called Alice rings [25–28].

In this work we report on a computational investigation of the solutions of two-component atomic BECs in a three-dimensional parabolic trap. The solutions are discovered with a numerical technique called deflation [29], which has been successfully applied to lower-dimensional or single-component systems [24, 30, 31], but has not been extended, to the best of our knowledge, to multi-component 3D problems. We complement this with a Bogolyubov-de Gennes (BdG) stability analysis and transient numerical simulations. Surprisingly, and contrary to what was found to be the case in the single-component setting [24, 30], the multi-component system allows for the *dynamically robust* existence of unexpected and highly complex vortical states, including ones featuring labyrinthine patterns. This suggests the potential observability of the obtained states.

Setup & Method.—A mixture of two bosonic components of the same atom species can be described, at the mean-field level, by a system of two coupled Gross–Pitaevskii (GP) equations [7, 8]. We refer to the two components as $-$ and $+$, and describe their distributions by the wave-functions $\Phi_\pm : D \times \mathbb{R}^+ \to \mathbb{C}$ with spatial domain $D = [-6, 6]^3 \subset \mathbb{R}^3$. The model can be written in its non-dimensional form as [4]:

$$i\frac{\partial \Phi_-}{\partial t} = -\frac{1}{2}\nabla^2\Phi_- + (g_{11}|\Phi_-|^2 + g_{12}|\Phi_+|^2)\Phi_- + V(\mathbf{r})\Phi_-,$$
$$i\frac{\partial \Phi_+}{\partial t} = -\frac{1}{2}\nabla^2\Phi_+ + (g_{12}|\Phi_-|^2 + g_{22}|\Phi_+|^2)\Phi_+ + V(\mathbf{r})\Phi_+,$$

with homogeneous Dirichlet boundary conditions on the boundary of the domain D. The symmetric 2×2 coefficient matrix $(g_{ij})_{1\leq i,j\leq 2}$ characterizes the interactions between the two components. Focusing on the case of the hyperfine states of ^{87}Rb, we use the parameter values $g_{11} = 100.4/98.006$, $g_{12} = 1$, and $g_{22} = 95.44/98.006$, proposed in [32, Table 2]. The function $V(\mathbf{r}) = \frac{1}{2}\Omega^2|\mathbf{r}|^2$ is a parabolic external confining spherical potential with strength $\Omega = 1$, where $|\mathbf{r}|^2 = x^2 + y^2 + z^2$. We compute stationary solutions to the coupled GP equations by assuming the standing wave ansatz $\Phi_\pm(\mathbf{r}, t) = \phi_\pm(\mathbf{r})e^{-i\mu_\pm t}$, and solving the following system of coupled

equations:

$$-\frac{1}{2}\nabla^2\phi_- + (g_{11}|\phi_-|^2 + g_{12}|\phi_+|^2)\phi_- + V(\mathbf{r})\phi_- - \mu_-\phi_- = 0,$$
$$-\frac{1}{2}\nabla^2\phi_+ + (g_{12}|\phi_-|^2 + g_{22}|\phi_+|^2)\phi_+ + V(\mathbf{r})\phi_+ - \mu_+\phi_+ = 0. \quad (1)$$

We discretize the real and imaginary components of ϕ_- and ϕ_+ using cubic Lagrange finite elements defined on a hexahedral mesh, with ten cells along each axis. The use of a hexahedral mesh is desirable because the discretized problem inherits some of the reflective symmetries of the infinite-dimensional problem. Eq. (1) is solved using the Firedrake finite element library [33] by combining Newton's method with the MUMPS LU solver [34] via PETSc [35] to solve the resulting linear equations.

We compute multiple solutions to Eq. (1) at parameters $(\mu_-, \mu_+) = (4, 5)$ using *deflation* [29]. Deflation allows us to identify new stationary solutions by modifying the nonlinear problem solved to prevent the discovery of known solutions by Newton's method. If $F(\phi_-, \phi_+)$ denotes the coupled NLS operator associated with Eq. (1) and (ϕ_{1-}, ϕ_{1+}) is a steady-state already obtained, then we construct and solve a new problem $G(\phi_-, \phi_+) = \mathcal{M}_1(\phi_-, \phi_+)F(\phi_-, \phi_+)$. The deflation operator $\mathcal{M}_1$ we employ is

$$\mathcal{M}_1 = \left(\frac{1}{\||\phi_-|^2 - |\phi_{1-}|^2\|^2} + 1\right)\left(\frac{1}{\||\phi_+|^2 - |\phi_{1+}|^2\|^2} + 1\right),$$

where $\|\cdot\|$ is the $H^1(D)$-norm. This operator prevents the convergence of Newton's method applied to G to the previous solution (ϕ_{1-}, ϕ_{1+}) (or its multiple by $e^{i\theta}$ for any $\theta \in \mathbb{R}$) since $\mathcal{M}_1(\phi_-, \phi_+) \to \infty$ as (ϕ_-, ϕ_+) approaches $e^{i\theta}(\phi_{1-}, \phi_{1+})$. This operator differs significantly from the one previously used in the single component setting [24] because it also deflates $(\phi_{1-}, 0)$ and $(0, \phi_{1+})$ to reduce the number of uninteresting solutions obtained. The deflation procedure can be iterated to deflate an arbitrary number of known solutions $\{(\phi_{i-}, \phi_{i_+})\}_{i=1}^n$ by constructing a problem $G = \mathcal{M}_n \cdots \mathcal{M}_1 F$.

Given the computational difficulty of the problem, a key challenge is to initialize our search with suitable initial guesses to discover a large number of solutions with complex patterns. Contrary to the single-component setting [24], we found that exploiting linear low-density limits of the system (1) is not an efficient strategy as it requires a large number of Newton iterations to eventually converge and results in simple steady-states. To achieve our goal of discovering complex but experimentally observable solutions (see the discussion of their stability below), we provided Newton's method with a large number of initial guesses of the form $(\phi_-, \phi_+) = (\phi_{7/2}, \phi_{9/2})$ by combining solutions to the nonlinear one-component equation. Here $\phi_{7/2}$ and $\phi_{9/2}$ are steady-states of the one-component problem emanating from the third and fourth excited states at chemical potential $\mu = 7/2$ and $\mu = 9/2$ previously discovered in [24].

Numerical Results.—We now illustrate some solutions discovered with deflation. Our procedure leads to the discovery of 150 distinct solutions to (1) with complex structures. We then conducted a BdG stability analysis (for which details can be found in the Supplementary Material). If the latter features imaginary or complex eigenfrequencies, the corresponding imaginary part $\omega_i \equiv \mathcal{I}(\omega)$ provides the instability's growth rate. Guided by this BdG stability analysis, we focus on the most physically relevant ones and partition our findings into three broad categories. The first set of our results is shown in Fig. 1 and captures a palette of unstable states partially identified in earlier works on one-component 3D systems. This illustrates that already some complex building blocks can be assembled into relevant stationary two-component solutions that the method can identify *without prior knowledge* of associated theoretical or numerical constructions.

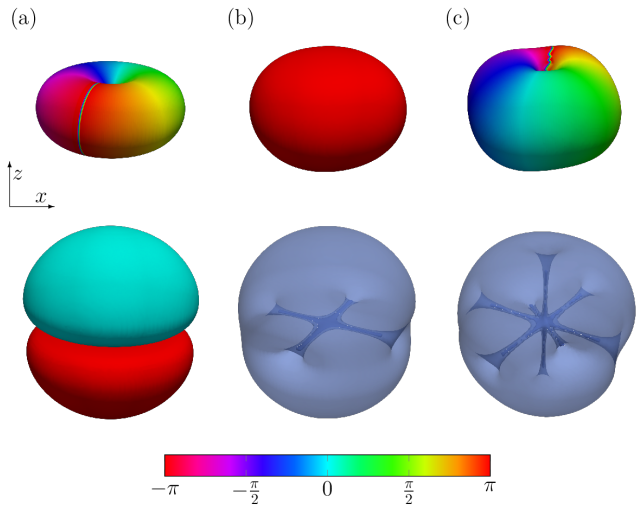

FIG. 1. Selection of three unstable steady-states whose individual components have been identified in previous works on the one-component GP equation. The top (resp. bottom) row illustrates the $-$ (resp. $+$) component of the solution. The colors represent the argument of the solution at isocontour of magnitude 0.2. Whenever appropriate, we display the density isosurfaces at densities 0.2 to visualize the vortex structure of the component.

We recognize in Fig. 1(a) a dipole solitary wave in the second component coupled with a vortical pattern in the first component. It is helpful to utilize a Cartesian notation $|k, m, n\rangle$, highlighting the number of nodes that exist in each x, y, z direction, to classify these states as a superposition of eigenstates near the linear limit. In that notation, the first component consists (at low density, i.e., near the linear limit) of $|1, 0, 0\rangle + i|0, 1, 0\rangle$, while the second one represents $|0, 0, 1\rangle$. This state is unstable with a growth rate of $\omega_i \approx 0.81$. Similarly un-

stable ($\omega_i \approx 0.30$) in panel (b) is a so-called Chladni soliton [23, 36] of a one-species condensate in the second component, coupled to a "ground state" (a nodeless cloud) in the first component. Finally, panel (c) reveals a single vortex pattern similar to panel (a) in the first component, while the second is an example of a star pattern, reminiscent of the ones described in [24, 37], with the following linear combination close to the linear limit: $|2,0,0\rangle - |0,2,0\rangle + i[|2,0,0\rangle - |0,0,2\rangle]$. This state has a growth rate of $\omega_i \approx 0.26$ and is unstable.

Dynamically stable states.—A more elaborate set of dynamically stable states has been identified and presented in Fig. 2. Here, we illustrate three distinct states identified as spectrally stable over *wide* parametric regimes. More specifically, the parameter regime we investigate is to linearly interpolate both chemical potentials, μ_- and μ_+, towards their low-density limits at μ_{0-} and μ_{0+} ($(\mu_{0-}, \mu_{0+}) = (1.5, 3.5)$ in Fig. 2(a) and $(3.5, 4.5)$ in Fig. 2(b,c)). Some of the resulting (widely) stable states are straightforward to interpret. For instance, in panel (a), we find a stable vortex star in the second component [37] coupled to a ground state of the first component. Two other stable states with simple configurations are depicted in Fig. 1 of the Supplementary Material.

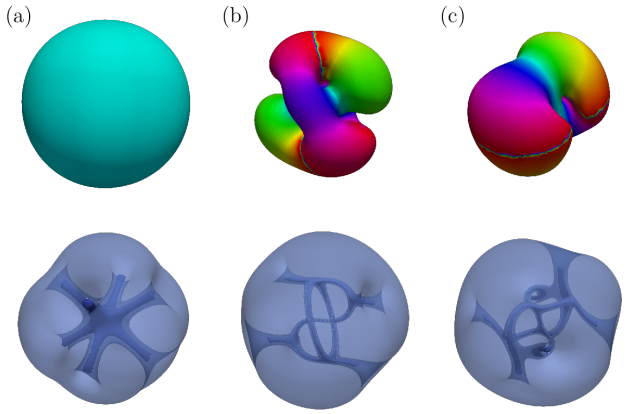

FIG. 2. Selection of three stable states to the NLS system with complex vortex structure on the second component (bottom row).

While one can argue that the above states are perhaps ones that can be expected in the two-component realm based on our single-component experience, this is far from obvious in the context of panels (b) and (c) of Fig. 2. The structure of panel (b) contains, in turn, two vortex lines in the first component that are coupled to a second component featuring an S-shaped vortex attached to a vortex ring, as well as two additional U-shaped vortex lines. Interestingly, such a state in a single-component was also obtained in our previous work [24] and was weakly unstable with a growth rate of $\omega_i \approx 5 \times 10^{-2}$

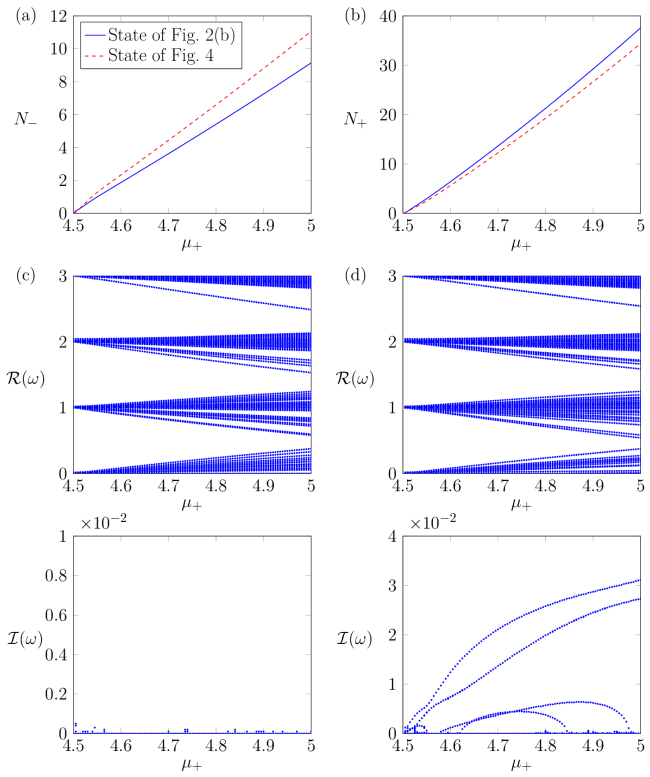

FIG. 3. Continuation and stability analysis of the states presented in Figs. 2(b) and 4 (at time $T = 0$) to the linear (low-density) limit as the chemical potentials (μ_-, μ_+) linearly approach $(3.5, 4.5)$. Panels (a) and (b) report the atomic numbers (N_-, N_+) of the components of the states illustrated in Fig. 2(b) (blue solid line) and Fig. 4 (red dashed line) as a function of the chemical potentials. Panels (c) and (d) respectively showcase the stability and weak instability of the states of Figs. 2(b) and 4.

at $\mu = 5$, illustrating that coupled systems may stabilize BEC configurations. Fig. 2(c) represents an especially complex, topologically charged configuration, where the vortex ring of the first component connects to an antisymmetric pattern reminiscent of a pair of vortex-based slings, each held by a vortex line. Importantly, despite the elaborate multi-vortical structure of these two configurations, our computations identify them as a spectrally and dynamically stable. As an illustration, we report in Fig. 3(a,b) the continuation of the atomic numbers (N_-, N_+) for each of the two components of the state presented in Fig. 2(b) as a function of the chemical potential μ_+. The real part of the relevant eigenfrequencies in the bottom left panel of Fig. 3(c) showcase the excitation frequencies, while the absence of imaginary eigenfrequencies (for most parameter values) in the bottom right panel indicates stability in our BdG analysis. This analysis is performed for all the stable states discussed above and further analyzed in the Supplementary Material.

Weakly unstable states.—In addition to these stable states, our deflation search yields a considerable wealth of weakly unstable states such as the one shown in Fig. 4 at time $T = 0$. Here, we observe a pair of vortex lines in the first component, coupled to a labyrinthine network involving multiple vortex rings, as well as S-shaped and U-shaped vortices (see the bottom row). Remarkably given the complexity of the state, yet in line with the BdG stability analysis, our dynamical simulations [38], involving hundreds of oscillation periods of the trap, identifies the state as only very weakly unstable, with a particularly small growth rate of $\omega_i \approx 3.1 \times 10^{-2}$ (see Figs. 3(d) and 4, and the movie in the Supplementary Material). This is only one of many such states that our detailed time-integration simulations, which conserve $N_\pm$ and the energy to machine precision, appear to preserve over time scales that would be relevant for experimental observability. Indeed, we present in Fig. 5 a selection of exotic weakly unstable states whose vortex structures involve structures well beyond the complexity of simple vortex rings and lines and rather extend to labyrinthine patterns of connected vorticity isocontours. The structures are sustained over a long time period with growth rates bounded by $\omega_i < 6.7 \times 10^{-2}$ at chemical potential values $(\mu_-, \mu_+) = (4, 5)$. Despite their complexity, all of these configurations are expected to be experimentally observable following our spectral stability analysis.

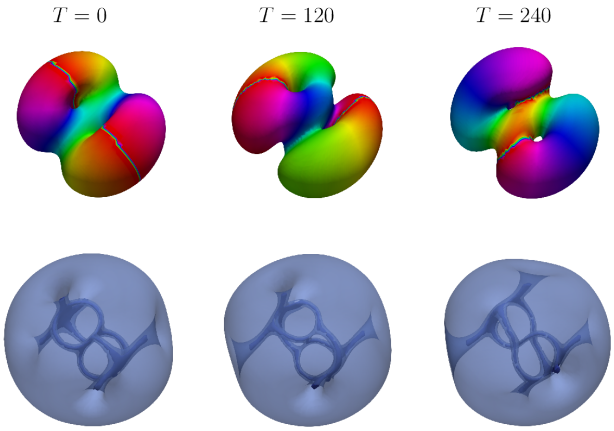

FIG. 4. Snapshots of the time evolution of a weakly unstable state, initially perturbed along its most unstable eigendirection. The top and bottom rows respectively display the first and second components of the state.

Conclusions & Future Work.—We have discovered a wealth of complex states to the two-component 3D GP equations. The deflation approach allowed us to retrieve a number of states that, to the best of our knowledge, had not been obtained previously, despite extensive efforts in this direction [4, 21, 22]. Even more importantly, several configurations involving combined vortical patterns, such as ones with S-shaped, U-shaped, and ring-shaped vortex

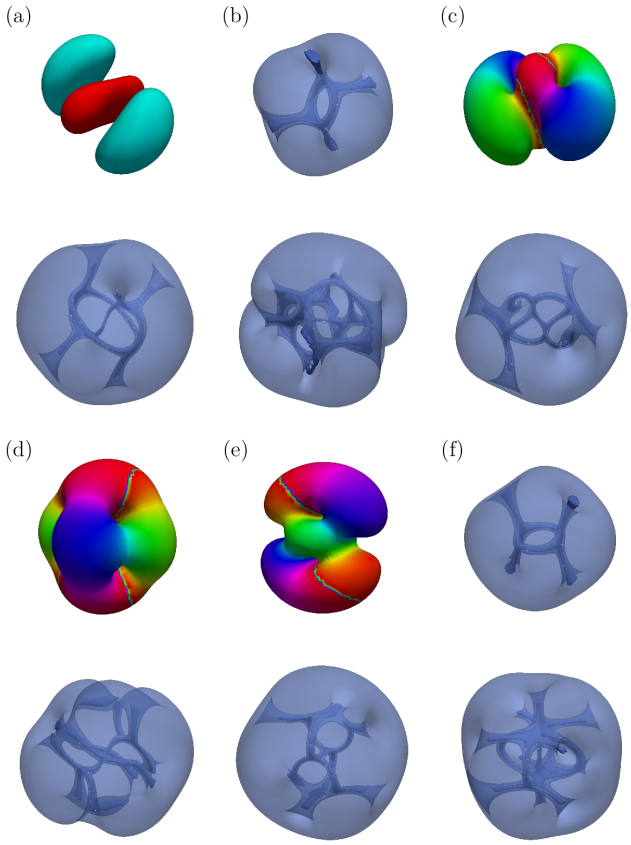

FIG. 5. Exotic weakly unstable solutions discovered by deflation which are within windows of experimental observability with growth rate $\omega_r < 6.7 \times 10^{-2}$.

patterns were found to be stable and, hence potentially accessible by state-of-the-art experimental techniques.

Our deflation technique enables the identification of complex (and possibly topologically-charged) patterns in a variety of nonlinear, elliptic partial differential equation problems of the Schrödinger class. The results were proposed in the experimentally tractable platform of atomic Bose–Einstein condensates. However, other settings where the nonlinear Schrödinger equation is relevant can be equally well applicable. In fact, the same numerical techniques could be broadly applicable to a variety of other problems, such as reaction-diffusion ones [39], among others.

The present work paves the way for numerous further possibilities. On the one hand, the theoretical understanding of such complex states, including from the linear limit of small amplitude, is a feature which has been explored in 1D and 2D settings [4], but not systematically in the 3D case, to the best of our knowledge. This is due to the computational complexity of the problem. Furthermore, while we have restricted our attention to the two-component pseudo-spinor case in this work, a significant volume of experiments has been recently fo-

cusing on 3-component spinor settings [20, 22]. It would be particularly interesting to extend the ideas presented herein in the latter setting.

Acknowledgments. This work is supported by the EPSRC Centre For Doctoral Training in Industrially Focused Mathematical Modelling (EP/L015803/1) in collaboration with Simula Research Laboratory (N.B.) and a London Mathematical Society Undergraduate Research Bursary URB-2021-21 (I.N.). This material is based upon work supported by the UK Engineering and Physical Sciences Research Council under Grants EP/W026163/1 and EP/R029423/1 (P.E.F.) and the US National Science Foundation under Grants No. PHY-2110030 (P.G.K.). The authors are particularly grateful to Prof. E. Charalampidis for his insights and earlier collaboration.

* boulle@maths.ox.ac.uk
† newell@maths.ox.ac.uk
‡ patrick.farrell@maths.ox.ac.uk
§ kevrekid@math.umass.edu

[1] C. Sulem and P. L. Sulem, *The nonlinear Schrödinger equation: self-focusing and wave collapse* (Springer, New York, 1999).
[2] M. Ablowitz, B. Prinari, and A. Trubatch, *Discrete and continuous nonlinear Schrödinger systems* (Cambridge University Press, Cambridge, 2004).
[3] M. J. Ablowitz, *Nonlinear dispersive waves* (Cambridge University Press, Cambridge, 2011).
[4] P. G. Kevrekidis, D. J. Frantzeskakis, and R. Carretero-González, *The defocusing nonlinear Schrödinger equation: from dark solitons to vortices and vortex rings* (SIAM, Philadelphia, PA, 2015).
[5] Y. S. Kivshar and G. P. Agrawal, *Optical solitons: From fibers to photonic crystals* (Academic Press, 2003).
[6] E. Infeld and G. Rowlands, *Nonlinear waves, solitons and chaos* (Cambridge University Press, Cambridge, 1990).
[7] C. J. Pethick and H. Smith, *Bose–Einstein condensation in dilute gases* (Cambridge University Press, Cambridge, 2002).
[8] S. Stringari and L. P. Pitaevskii, *Bose–Einstein condensation* (Oxford University Press, Oxford, 2003).
[9] F. K. Abdullaev, A. Gammal, A. M. Kamchatnov, and L. Tomio, Dynamics of bright matter wave solitons in a Bose–Einstein condensate, Int. J. Mod. Phys. B **19**, 3415 (2005).
[10] D. J. Frantzeskakis, Dark solitons in atomic Bose–Einstein condensates: from theory to experiments, J. Phys. A-Math. Theor. **43**, 213001 (2010).
[11] A. L. Fetter and A. A. Svidzinsky, Vortices in a trapped dilute Bose–Einstein condensate, J. Phys.-Condens. Mat. **13**, R135 (2001).
[12] A. L. Fetter, Rotating trapped Bose–Einstein condensates, Rev. Mod. Phys. **81**, 647 (2009).
[13] S. Komineas, Vortex rings and solitary waves in trapped Bose–Einstein condensates, Eur. Phys. J.-Spec. Top. **147**, 133 (2007).
[14] D. Kleckner and W. T. M. Irvine, Creation and dynamics of knotted vortices, Nat. Phys. **9**, 253 (2013).
[15] D. S. Hall, M. W. Ray, K. Tiurev, E. Ruokokoski, A. H. Gheorghe, and M. Möttönen, Tying quantum knots, Nat. Phys. **12**, 478 (2016).
[16] C. Ryu, M. F. Andersen, P. Cladé, V. Natarajan, K. Helmerson, and W. D. Phillips, Observation of persistent flow of a Bose–Einstein condensate in a toroidal trap, Phys. Rev. Lett. **99**, 260401 (2007).
[17] M. C. Tsatsos, P. E. Tavares, A. Cidrim, A. R. Fritsch, M. A. Caracanhas, F. E. A. dos Santos, C. F. Barenghi, and V. S. Bagnato, Quantum turbulence in trapped atomic Bose–Einstein condensates, Phys. Rep. **622**, 1 (2016).
[18] S. Eckel, A. Kumar, T. Jacobson, I. B. Spielman, and G. K. Campbell, A rapidly expanding Bose–Einstein condensate: an expanding universe in the lab, Phys. Rev. X **8**, 021021 (2018).
[19] V. Kolobov, K. Golubkov, J. Muñoz de Nova, and J. Steinhauer, Observation of stationary spontaneous Hawking radiation and the time evolution of an analogue black hole, Nat. Phys. **17**, 362 (2021).
[20] D. M. Stamper-Kurn and M. Ueda, Spinor bose gases: Symmetries, magnetism, and quantum dynamics, Rev. Mod. Phys. **85**, 1191 (2013).
[21] P. G. Kevrekidis and D. J. Frantzeskakis, Solitons in coupled nonlinear Schrödinger models: A survey of recent developments, Rev. Phys. **1**, 140 (2016).
[22] Y. Kawaguchi and M. Ueda, Spinor Bose–Einstein condensates, Phys. Rep. **520**, 253 (2012).
[23] A. M. Mateo and J. Brand, Stability and dispersion relations of three-dimensional solitary waves in trapped Bose–Einstein condensates, New J. Phys. **17**, 125013 (2015).
[24] N. Boullé, E. G. Charalampidis, P. E. Farrell, and P. G. Kevrekidis, Deflation-based identification of nonlinear excitations of the three-dimensional Gross-Pitaevskii equation, Phys. Rev. A **102**, 053307 (2020).
[25] J. Lovegrove, M. O. Borgh, and J. Ruostekoski, Energetically stable singular vortex cores in an atomic spin-1 Bose–Einstein condensate, Phys. Rev. A **86**, 013613 (2012).
[26] J. Lovegrove, M. O. Borgh, and J. Ruostekoski, Stability and internal structure of vortices in spin-1 Bose–Einstein condensates with conserved magnetization, Phys. Rev. A **93**, 033633 (2016).
[27] T. Mithun, R. Carretero-González, E. G. Charalampidis, D. S. Hall, and P. G. Kevrekidis, Existence, stability, and dynamics of monopole and Alice ring solutions in antiferromagnetic spinor condensates, Phys. Rev. A **105**, 053303 (2022).
[28] J. Ruostekoski and J. R. Anglin, Monopole core instability and Alice rings in spinor Bose–Einstein condensates, Phys. Rev. Lett. **91**, 190402 (2003).
[29] P. E. Farrell, A. Birkisson, and S. W. Funke, Deflation techniques for finding distinct solutions of nonlinear partial differential equations, SIAM J. Sci. Comput. **37**, A2026 (2015).
[30] E. G. Charalampidis, P. G. Kevrekidis, and P. E. Farrell, Computing stationary solutions of the two-dimensional Gross–Pitaevskii equation with deflated continuation, Commun. Nonlinear Sci. Numer. Simulat. **54**, 482 (2018).
[31] E. G. Charalampidis, N. Boullé, P. E. Farrell, and P. G. Kevrekidis, Bifurcation analysis of stationary solutions of two-dimensional coupled Gross-Pitaevskii equations us-

ing deflated continuation, Commun. Nonlinear Sci. Numer. Simulat. **87**, 105255 (2020).

[32] M. Egorov, B. Opanchuk, P. Drummond, B. Hall, P. Hannaford, and A. Sidorov, Measurement of s-wave scattering lengths in a two-component Bose-Einstein condensate, Phys. Rev. A **87**, 053614 (2013).

[33] F. Rathgeber, D. A. Ham, L. Mitchell, M. Lange, F. Luporini, A. T. McRae, G.-T. Bercea, G. R. Markall, and P. H. Kelly, Firedrake: automating the finite element method by composing abstractions, ACM Trans. Math. Softw. **43**, 1 (2016).

[34] P. R. Amestoy, I. S. Duff, J. Koster, and J.-Y. L'Excellent, A fully asynchronous multifrontal solver using distributed dynamic scheduling, SIAM J. Matrix Anal. Appl. **23**, 15 (2001).

[35] S. Balay, S. Abhyankar, M. F. Adams, S. Benson, J. Brown, P. Brune, K. Buschelman, E. Constantinescu, L. Dalcin, A. Dener, *et al.*, *PETSc/TAO Users Manual*, Tech. Rep. ANL-21/39 - Revision 3.17 (Argonne National Laboratory, 2022).

[36] A. M. Mateo and J. Brand, Chladni solitons and the onset of the snaking instability for dark solitons in confined superfluids, Phys. Rev. Lett. **113**, 255302 (2014).

[37] L.-C. Crasovan, V. M. Pérez-García, I. Danaila, D. Mihalache, and L. Torner, Three-dimensional parallel vortex rings in Bose–Einstein condensates, Phys. Rev. A **70**, 033605 (2004).

[38] M. Delfour, M. Fortin, and G. Payre, Finite-difference solutions of a non-linear Schrödinger equation, J. Comput. Phys. **44**, 277 (1981).

[39] J. Smoller, *Shock waves and reaction–diffusion equations* (Springer-Verlag, New York, 1983).

Supplementary Material for "Two-Component 3D Atomic Bose-Einstein Condensates Support Complex Stable Patterns"

N. Boullé,[1,*] I. Newell,[1,†] P. E. Farrell,[1,‡] and P. G. Kevrekidis[2,§]

[1] *Mathematical Institute, University of Oxford, Oxford OX2 6GG, United Kingdom*
[2] *Department of Mathematics and Statistics, University of Massachusetts Amherst, Amherst, MA 01003-4515, USA*

STABLE STATES AND CONTINUATION

As described in the main text, deflation identified five stable, topologically charged solutions to the nonlinear Schrödinger system (NLS) at chemical potentials $(\mu_-, \mu_+) = (4, 5)$. The two states which are not analyzed in the paper are displayed in Fig. 1. Fig. 1(a) features a fundamental state in the first component that is complemented by a vortex of topological charge $l = 2$ in the second component. Fig. 1(b) shows a vortex of topological charge $l = 1$ in the second component harboring an effective bright soliton within a vortex-bright line configuration [1]. As we will see in the next section and Fig. 2(c,d), these states are stable over a wide parametric regime of the chemical potentials up to the linear (low-density) limit.

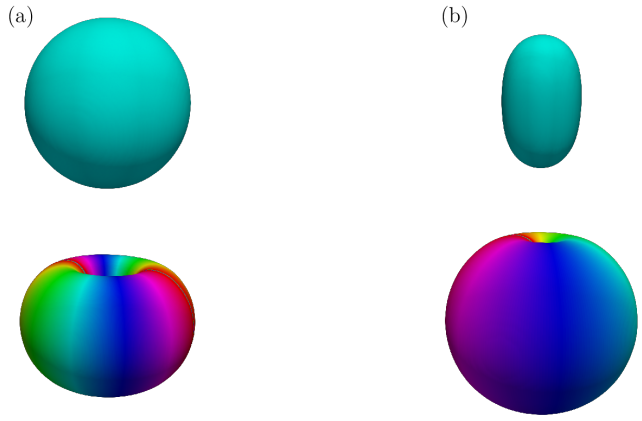

FIG. 1. The two remaining stable states to the NLS system discovered by deflation (in addition to those shown in Fig. 2 of the main manuscript). The top (resp. bottom) row illustrates the - (resp. +) component of the solution. The colors represent the argument of the solution at isocontour of magnitude 0.2.

Once a steady state has been discovered by deflation at parameters $(\mu_-, \mu_+) = (4, 5)$, we continue it to the linear limit at (μ_{0-}, μ_{0+}) by performing a linear interpolation in both components. As μ_+ (the chemical potential of the first component) decreases from $\mu_{\text{init}+}$ to μ_{0+}, we want μ_- (the chemical potential of the second component) to vary from $\mu_{\text{init}-}$ to μ_{0-}. This yields the following linear interpolation equation for μ_-:

$$\mu_- = \mu_{\text{init}-} \frac{\mu_+ - \mu_{0+}}{\mu_{\text{init}+} - \mu_{0+}} + \mu_{0-} \frac{\mu_{\text{init}+} - \mu_+}{\mu_{\text{init}+} - \mu_{0+}}. \tag{1}$$

After identifying the chemical potential parameters μ_{0-} and μ_{0+} at which the two components emerge, we then discretize the interval $[\mu_{0+}, \mu_{\text{init}+}]$ with regular step-size $\Delta\mu = 10^{-2}$, where $\mu_{\text{init}+} = 5$. A steady state is continued to the linear limit as μ_+ goes from $\mu_{\text{init}+} \to \mu_{0+}$ (and similarly for μ_- using Eq. (1)) by solving the NLS system using the solution at the previous step in the chemical potential as initial guess. We then display the continuation of the state (ϕ_-, ϕ_+) by reporting the atomic number of each component:

$$N_- = \int_\Omega |\phi_-|^2 \, \mathrm{d}x, \qquad N_+ = \int_\Omega |\phi_+|^2 \, \mathrm{d}x,$$

as a function of the parameter μ_+. As the state is continued towards the low-density limit at (μ_{0-}, μ_{0+}), the atomic numbers N_- and N_+ converge to zero.

STABILITY ANALYSIS

We now provide more details about the stability computations of the discovered solutions to the time-dependent NLS system

$$\begin{aligned} i\frac{\partial \Phi_-}{\partial t} =& -\frac{1}{2}\nabla^2\Phi_- + (g_{11}|\Phi_-|^2 + g_{12}|\Phi_+|^2)\Phi_- + V(\mathbf{r})\Phi_-, \\ i\frac{\partial \Phi_+}{\partial t} =& -\frac{1}{2}\nabla^2\Phi_+ + (g_{12}|\Phi_-|^2 + g_{22}|\Phi_+|^2)\Phi_+ + V(\mathbf{r})\Phi_+. \end{aligned} \tag{2}$$

Once a steady-state $\phi_\pm^0(\mathbf{r})$ to Eq. (2) has been identified by deflation, we perform a Bogolyubov–de Gennes (BdG) spectral stability analysis [2–4] by using the following perturbation ansatz [5],

$$\begin{aligned} \widetilde{\Phi}_-(\mathbf{r},t) &= e^{-i\mu_- t}\left[\phi_-^0 + \varepsilon\left(a(\mathbf{r})e^{i\omega t} + b^*(\mathbf{r})e^{-i\omega^* t}\right)\right], \\ \widetilde{\Phi}_+(\mathbf{r},t) &= e^{-i\mu_+ t}\left[\phi_+^0 + \varepsilon\left(c(\mathbf{r})e^{i\omega t} + d^*(\mathbf{r})e^{-i\omega^* t}\right)\right], \end{aligned} \tag{3}$$

where $\omega \in \mathbb{C}$ is the eigenfrequency, $\varepsilon \ll 1$ is a small parameter, and $*$ denotes the complex conjugate. Inserting this equation into Eq. (2) yields an eigenvalue problem at order $\mathcal{O}(\epsilon)$, which we write in matrix form as

$$\begin{pmatrix} A_{11} & A_{12} & A_{13} & A_{14} \\ -A_{12}^* & -A_{11} & -A_{14}^* & -A_{13}^* \\ A_{13}^* & A_{14} & A_{33} & A_{34} \\ -A_{14}^* & -A_{13} & -A_{34}^* & -A_{33} \end{pmatrix} \begin{pmatrix} a \\ b \\ c \\ d \end{pmatrix} = \rho \begin{pmatrix} a \\ b \\ c \\ d \end{pmatrix}, \tag{4}$$

with eigenvalue $\rho = -\omega$ and eigenvector $\mathcal{V} = [a\, b\, c\, d]^\top$. The matrix elements in Eq. (4) are given by

$$\begin{aligned} A_{11} &= -\frac{1}{2}\nabla^2 + \left(2g_{11}|\phi_-^0|^2 + g_{12}|\phi_+^0|^2\right) + V(\mathbf{r}) - \mu_-, & A_{12} &= g_{11}\left(\phi_-^0\right)^2, \\ A_{33} &= -\frac{1}{2}\nabla^2 + \left(g_{12}|\phi_-^0|^2 + 2g_{22}|\phi_+^0|^2\right) + V(\mathbf{r}) - \mu_+, & A_{34} &= g_{22}\left(\phi_+^0\right)^2, \\ A_{13} &= g_{12}\,\phi_-^0\left(\phi_+^0\right)^*, & A_{14} &= g_{12}\,\phi_-^0\phi_+^0. \end{aligned}$$

Similar to [6], we decompose Eq. (4) into real and imaginary parts to solve the discretized 8×8 block matrix eigenvalue problem. We employ the same piecewise cubic finite element discretization as the one used for solving the NLS system and solve the resulting eigenvalue problem using a Krylov–Schur algorithm with a shift-and-invert spectral transformation implemented [7] in the Scalable Library for Eigenvalue Problem Computations (SLEPc) [8]. We then decompose the eigenfrequencies $\omega \in \mathbb{C}$ into real and imaginary parts as $\omega = \omega_r + i\omega_i$. A state is considered spectrally stable at the chemical potentials (μ_-, μ_+) if the eigenfrequencies have imaginary parts satisfying $|\omega_i| < 10^{-3}$. We report in panels (a) to (d) of Fig. 2 the atomic numbers and stability analysis of the stable states displayed in Fig. 2(a,c) of the main text and Fig. 1(a,b), respectively. We observe that all the five states identified by deflation described as stable in the main text are stable over a wide parametric regime of the chemical potentials, up to the linear limit.

DYNAMICAL SIMULATIONS

To verify the spectral stability or weak instability of a state $\phi_\pm^0$ discovered by deflation, we integrate the time-dependent NLS system (2) until $t = 240$ by perturbing $\phi_\pm^0$ along its most unstable eigendirection similarly to Eq. (3). We then select $\epsilon = 10^{-2}$ and use $\psi_\pm^{(0)}(\mathbf{r}) \coloneqq \tilde{\Phi}_\pm(\mathbf{r}, t=0)$ as initial state for the time-integration of the system. Let $\Delta t = 10^{-2}$ be the time-step and $\psi_\pm^{(n)}(\mathbf{r}) = \psi_\pm(\mathbf{r}, n\Delta t)$ be the solution to (2) at time $t_n = n\Delta t$. The time discretization of the system is performed using a modified Crank-Nicolson method [9] such that the solution $\psi_\pm^{(n+1)}$ at time t_{n+1} satisfies

$$i\frac{\psi_-^{(n+1)} - \psi_-^{(n)}}{\Delta t} = \left(-\frac{1}{2}\nabla^2 + V(\mathbf{r})\right)\tilde{\psi}_-^{(n)} + \left(g_{11}\frac{|\psi_-^{(n+1)}|^2 + |\psi_-^{(n)}|^2}{2} + g_{12}\frac{|\psi_+^{(n+1)}|^2 + |\psi_+^{(n)}|^2}{2}\right)\tilde{\psi}_-^{(n)}, \tag{5a}$$

$$i\frac{\psi_+^{(n+1)} - \psi_+^{(n)}}{\Delta t} = \left(-\frac{1}{2}\nabla^2 + V(\mathbf{r})\right)\tilde{\psi}_+^{(n)} + \left(g_{12}\frac{|\psi_-^{(n+1)}|^2 + |\psi_-^{(n)}|^2}{2} + g_{22}\frac{|\psi_+^{(n+1)}|^2 + |\psi_+^{(n)}|^2}{2}\right)\tilde{\psi}_+^{(n)}. \tag{5b}$$

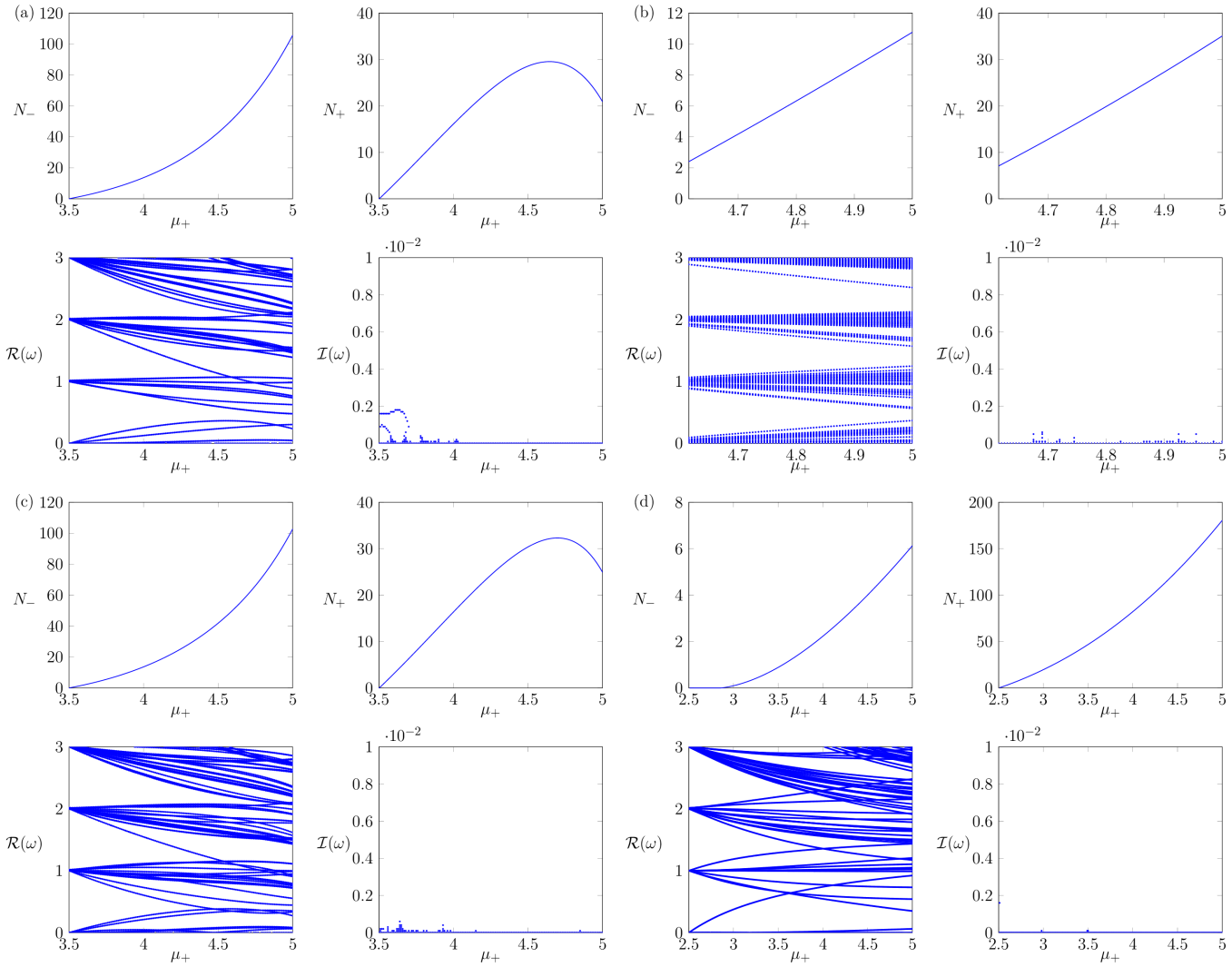

FIG. 2. Continuation and stability analysis of the states presented in Fig. 2(a,c) of the main text and Fig. 1 of the Supplementary Material in panels (a)-(d), respectively. Each panel features the atomic numbers (N_-, N_+) of the components of the state as well as the real and imaginary parts of the associated eigenfrequencies. The linear limit for the states presented in panels (a) to (d) are respectively $(\mu_-, \mu_+) \to (1.5, 3.5)$, $(3.5, 4.5)$, $(1.5, 3.5)$, and $(1.5, 2.5)$.

where $\tilde{\psi}_-^{(n)} = (\psi_-^{(n+1)} + \psi_-^{(n)})/2$ and $\tilde{\psi}_+^{(n)} = (\psi_+^{(n+1)} + \psi_+^{(n)})/2$.

As for the single component nonlinear Schrödinger equation [9], one can show that this time-stepping scheme conserves the atomic number of each component of the state, as well as the energy $\mathcal{E}$, defined as

$$\mathcal{E}(\psi_-, \psi_+) = \int_\Omega \frac{1}{4}\left(|\nabla\psi_-|^2 + |\nabla\psi_+|^2\right) + \frac{1}{2}V(\mathbf{r})(|\psi_-|^2 + |\psi_+|^2) + \frac{1}{4}g_{11}|\psi_-|^4 + \frac{1}{4}g_{22}|\psi_+|^4 + \frac{1}{2}g_{12}|\psi_-\psi_+|^2\,\mathrm{d}x. \quad (6)$$

Hence, multiplying Eqs. (5a) and (5b) by $\bar{\tilde{\psi}}_-^{(n)}$ and $\bar{\tilde{\psi}}_+^{(n)}$, taking the imaginary part, and integrating over the domain Ω yields the conservation of the atomic numbers since we obtain

$$\int_\Omega |\psi_-^{(n+1)}|^2\,\mathrm{d}x = \int_\Omega |\psi_-^{(n)}|^2\,\mathrm{d}x, \quad \text{and} \quad \int_\Omega |\psi_+^{(n+1)}|^2\,\mathrm{d}x = \int_\Omega |\psi_+^{(n)}|^2\,\mathrm{d}x.$$

We now show that the energy of the state is conserved by the time-stepping scheme. To do so, we first multiply Eqs. (5a) and (5b) by $(\bar{\psi}_-^{(n+1)} - \bar{\psi}_-^{(n)})$ and $(\bar{\psi}_+^{(n+1)} - \bar{\psi}_+^{(n)})$, take the real part of the resulting equations, and integrate

over the domain to obtain

$$-\frac{1}{4}\int_\Omega |\nabla\psi_-^{(n+1)}|^2 - |\nabla\psi_-^{(n)}|^2\,\mathrm{d}x - \frac{1}{2}\int_\Omega V(\mathbf{r})(|\psi_-^{(n+1)}|^2 - |\psi_-^{(n)}|^2)\,\mathrm{d}x = \frac{1}{4}\int_\Omega \left(g_{11}(|\psi_-^{(n+1)}|^2 + |\psi_-^{(n)}|^2) + g_{12}(|\psi_+^{(n+1)}|^2 + |\psi_+^{(n)}|^2)\right)\left(|\psi_-^{(n+1)}|^2 - |\psi_-^{(n)}|^2\right)\,\mathrm{d}x, \tag{7a}$$

$$-\frac{1}{4}\int_\Omega |\nabla\psi_+^{(n+1)}|^2 - |\nabla\psi_+^{(n)}|^2 dx - \frac{1}{2}\int_\Omega V(\mathbf{r})(|\psi_+^{(n+1)}|^2 - |\psi_+^{(n)}|^2)\,\mathrm{d}x = \frac{1}{4}\int_\Omega \left(g_{12}(|\psi_-^{(n+1)}|^2 + |\psi_-^{(n)}|^2) + g_{22}(|\psi_+^{(n+1)}|^2 + |\psi_+^{(n)}|^2)\right)\left(|\psi_+^{(n+1)}|^2 - |\psi_+^{(n)}|^2\right)\,\mathrm{d}x. \tag{7b}$$

The right-hand side of Eq. (7a) is equivalent to

$$\frac{1}{4}\int_\Omega \left(g_{11}(|\psi_-^{(n+1)}|^2 + |\psi_-^{(n)}|^2) + g_{12}(|\psi_+^{(n+1)}|^2 + |\psi_+^{(n)}|^2)\right)\left(|\psi_-^{(n+1)}|^2 - |\psi_-^{(n)}|^2\right)\,\mathrm{d}x =$$
$$\frac{1}{4}\int_\Omega g_{11}\left(|\psi_-^{(n+1)}|^4 - |\psi_-^{(n)}|^4\right) + g_{12}\left(|\psi_+^{(n+1)}\psi_-^{(n+1)}|^2 - |\psi_+^{(n)}\psi_-^{(n)}|^2 - |\psi_+^{(n+1)}\psi_-^{(n)}|^2 + |\psi_+^{(n)}\psi_-^{(n+1)}|^2\right)\,\mathrm{d}x.$$

Similarly, the right-hand side of Eq. (7b) yields

$$\frac{1}{4}\int_\Omega \left(g_{12}(|\psi_-^{(n+1)}|^2 + |\psi_-^{(n)}|^2) + g_{22}(|\psi_+^{(n+1)}|^2 + |\psi_+^{(n)}|^2)\right)\left(|\psi_+^{(n+1)}|^2 - |\psi_+^{(n)}|^2\right)\,\mathrm{d}x =$$
$$\frac{1}{4}\int_\Omega g_{22}\left(|\psi_+^{(n+1)}|^4 - |\psi_+^{(n)}|^4\right) + g_{12}\left(|\psi_+^{(n+1)}\psi_-^{(n+1)}|^2 - |\psi_+^{(n)}\psi_-^{(n)}|^2 - |\psi_-^{(n+1)}\psi_+^{(n)}|^2 + |\psi_-^{(n)}\psi_+^{(n+1)}|^2\right)\,\mathrm{d}x.$$

Therefore, after summing Eqs. (7a) and (7b), we find that the energy is conserved by the time-stepping scheme as $\mathcal{E}(\psi_-^{(n+1)}, \psi_+^{(n+1)}) = \mathcal{E}(\psi_-^{(n)}, \psi_+^{(n)})$.

* boulle@maths.ox.ac.uk
† newell@maths.ox.ac.uk
‡ patrick.farrell@maths.ox.ac.uk
§ kevrekid@math.umass.edu

[1] E. G. Charalampidis, W. Wang, P. G. Kevrekidis, D. J. Frantzeskakis, and J. Cuevas-Maraver, SO(2)-induced breathing patterns in multicomponent Bose–Einstein condensates, Phys. Rev. A **93**, 063623 (2016).
[2] C. J. Pethick and H. Smith, *Bose–Einstein condensation in dilute gases* (Cambridge University Press, Cambridge, 2002).
[3] S. Stringari and L. P. Pitaevskii, *Bose–Einstein condensation* (Oxford University Press, Oxford, 2003).
[4] P. G. Kevrekidis, D. J. Frantzeskakis, and R. Carretero-González, *The defocusing nonlinear Schrödinger equation: from dark solitons to vortices and vortex rings* (SIAM, Philadelphia, PA, 2015).
[5] E. G. Charalampidis, N. Boullé, P. E. Farrell, and P. G. Kevrekidis, Bifurcation analysis of stationary solutions of two-dimensional coupled Gross-Pitaevskii equations using deflated continuation, Commun. Nonlinear Sci. Numer. Simulat. **87**, 105255 (2020).
[6] N. Boullé, E. G. Charalampidis, P. E. Farrell, and P. G. Kevrekidis, Deflation-based identification of nonlinear excitations of the three-dimensional Gross-Pitaevskii equation, Phys. Rev. A **102**, 053307 (2020).
[7] G. W. Stewart, A Krylov–Schur algorithm for large eigenproblems, SIAM J. Matrix Anal. A. **23**, 601 (2002).
[8] V. Hernandez, J. E. Roman, and V. Vidal, SLEPc: A scalable and flexible toolkit for the solution of eigenvalue problems, ACM Trans. Math. Softw. **31**, 351 (2005).
[9] M. Delfour, M. Fortin, and G. Payre, Finite-difference solutions of a non-linear Schrödinger equation, J. Comput. Phys. **44**, 277 (1981).